ASTFE
American Society
of Thermal and Fluids Engineers

8th Thermal and Fluids Engineering Conference (TFEC)
March, 26-29, 2023
Partially Online Virtual and at University of Maryland, MD Conference

TFEC-2023-46031

CORRELATIONS AMONG CHARACTERISTICS OF GYROID-TYPE CELLULAR FOAM STRUCTURES

N. Bianco[1], M. Iasiello[1*], G. Scarpati[1], M. Bartlett[2], G. M. Mauro[3], A. Andreozzi[1], W. K. S. Chiu[2]

[1] Dipartimento di Ingegneria Industriale, Università degli Studi di Napoli Federico II, P.le Tecchio 80, 80125, Napoli, Italy
[2] Department of Mechanical Engineering, University of Connecticut, 191 Auditorium Road, Storrs, CT, 06269-3139, USA
[3] Dipartimento di Ingegneria, Università degli Studi del Sannio, P.za Roma 21, 82100, Benevento, Italy

ABSTRACT

Among cellular materials, Triply-Periodic Minimal Surfaces are promising for thermal management applications because of their high specific surface area, tortuosity, and effective thermal conductivity. In very recent years, additive manufacturing techniques are being employed in designing and printing customized 3D cellular structures, which allow to maximize their heat transfer performance. In applications where convection plays a significant role, monitoring pressure drop is important because of its contrasting role to convective heat transfer enhancement. A CFD analysis of pressure drop in air flowing through gyroid-type structures with different porosities and cell sizes is carried out and presented. Governing equations with appropriate boundary conditions are solved with a finite element commercial code. Velocity and pressure fields as well as correlations to predict the permeability and the Forchheimer coefficient, useful to designers of gyroid-type structures, are presented.

KEY WORDS: Porous media; Triply-Periodic Minimal Surfaces; Pressure drop; Permeability; Correlations.

1. INTRODUCTION

Because of their high surface area to volume ratio and tortuosity that promotes flow mixing, cellular materials are promising materials to be used in heat transfer applications, such as heat exchangers, thermal energy storage systems, heat sinks for electronics and so on [1]. When convective heat transfer is involved, pressure drop plays a main role and deserves attention, since it is often quite relevant. The effects of pressure drop in cellular structures are evaluated by permeability and Forchheimer coefficient, which depend on microstructure characteristics, such as porosity and cells size [2]. They can be obtained experimentally [3], as well as with predictive approaches, either by numerical simulations on pore-scale reconstructed cellular structures [4] or analytical solutions derived for simplified geometries [5]. Within predictive approaches, first pressure drop is obtained, and permeability and Forchheimer coefficient are then determined. Very recent additive manufacturing techniques allow to design and print cellular materials, such as Triply-Periodic Minimal Surfaces (TPMS), very suitable in heat transfer application, because of their excellent heat transfer area to volume ratio [6]. Cellular structures are engineered starting from well-established TPMSs, that are characterized by locally minimal surface area and zero mean curvature [7]. In recent years several studies were carried out to predict both pressure drop and permeability and to find correlations to monitor them. Pressure drop within eight different 0.80 porosity TPMS-based bone scaffold was computed to derive permeability by Ali et al. [8]. Permeability values in the 1 to 3 range, depending on the investigated TPMS, were derived. A 0.70 porosity TPMS, used as scaffold, was analyzed by Castro et al. [9], who showed that, also for smaller porosity, the TPMS structure played a relevant role on pressure drop and permeability. Convective heat transfer and pressure drop in Gyroid and Schwarz-P TPMSs were investigated by Kaur and Singh [10] and compared against a conventional Kelvin's foam. Results showed that Gyroid TPMSs exhibited a better thermal

*Corresponding Author: marcello.iasiello@unina.it

performance, at equal pumping power. Heat transfer coefficient, flow resistance, and structural strength of various TPMSs were evaluated and compared by Cheng et al. [11]. The authors claimed that the investigated TPMSs performed better than conventional sintered metal particle structures. Several models for the prediction of the permeability have been proposed through the years [12, 13]. Zhianmanesh et al. [12], starting from computational simulations, derived a set of correlations between permeability and porosity for different kinds of TPMSs, employing a second-order polynomial fit, with higher than 0.99 coefficients of determination. The dependence of the permeability on the pore size of the structure was investigated by Asbai-Ghoudan et al. [13]. The authors presented correlations among pore size and porosity values, obtained via CFD simulations, for Gyroid, Fisher-Kock, and Schwarz P. TPMSs. However, presently, no correlations between permeability and Forchheimer coefficient for high Reynolds number are available in the open literature.

In the present work, permeability and Forchheimer coefficient are correlated with porosity and cell size, for a Gyroid TPMS microstructure. After performing computations to obtain pressure drops, permeability and Forchheimer coefficient are evaluated via data reduction. The permeability is first assumed to be proportional to the square of the cell size and, then, by means of a linear regression analysis, it is correlated with the porosity. On the other hand, a generic power law is employed to correlate the Forchheimer coefficient with both porosity and cell size. The derived set of correlations will be helpful in the investigation of pressure drop in TPMS-based manufactured engineering devices.

2. MATHEMATICAL MODEL

2.1 Structure generation

Structure generation was performed by MSLattice. A basic property of TPMS structures is that they are defined through the use of a combination of trigonometric functions $\phi(x, y, z)$, which allows for great control when designing novel TPMS structures. The MSLattice design parameters of interest were solid volume fraction and TPMS type, which modify $\phi(x, y, z)$. MSLattice achieved structure generation through the creation of a sheet-network lattice by defining a solid area normal to and antinormal to $\phi(x, y, z)$. This sheet-network lattice was then used to find the solid area by solving the equation $-c \leq \phi(x, y, z) \leq c$ [14]. The TPMS structure was then exported as a .STL file. The COMSOL CAD Toolbox was used to import the generated TPMS .STL file into COMSOL Multiphysics directly for use in CFD. A Boolean inverse operation was performed on the solid TPMS structure to define the fluid domain. Inflow and outflow boxes were added to allow flow to develop before interacting with the TPMS structure. The inflow/outflow lengths are half the overall length of the TPMS structure. The fluid domain of the investigated Gyroid TPMS structure with inflow and outflow boxes is sketched in Fig. 1a; the boundary conditions are reported in Fig. 1b.

2.2 Mathematical modeling

To identify the flow regime, the Reynolds number was used and calculated by the equation:

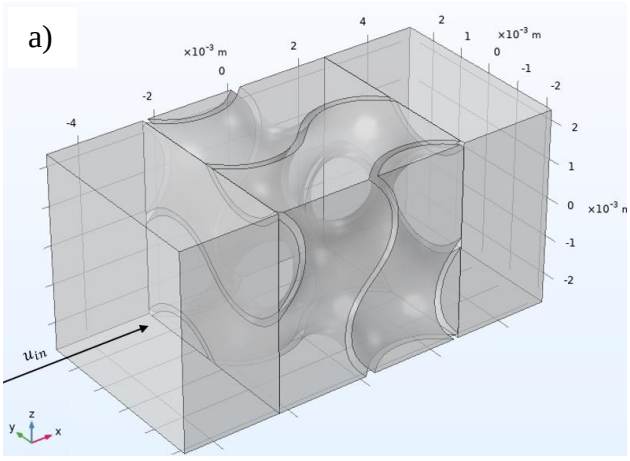

b)

At the inlet section $x = -\frac{1}{2} d_c$, $\overline{u} = -u_{in}\hat{n}$

At the outlet section $x = \frac{3}{2} d_c$, $p = 0$

At the side faces $y = z = 0$ and $y = z = d_c$, $\overline{u} \cdot \hat{n} = 0$

At the air-TPMS interfaces, $\overline{u} = 0$

Fig. 1 a) The domain of the investigated structure with inflow and outflow boxes; b) boundary conditions.

$$\mathrm{Re} = \frac{\text{Inertial forces}}{\text{Viscous forces}} = \frac{\rho\, u_{in}\, D_h}{\mu} \tag{1}$$

where ρ and μ are the density and the dynamic viscosity of the fluid evaluated at the inlet section of the cell domain, u_{in} is the fluid inlet velocity and D_h is the hydraulic diameter evaluated as $D_h = 4\,\varepsilon\,V/S$, where ε is the porosity of the structure, V is the volume of the cell (solid-fluid) domain and S is the solid-fluid interface surface area. In all the simulations the flow was considered always laminar (Re < 600) [15]).

Governing equations. The conservation of mass and conservation of momentum are satisfied throughout the whole fluid domain. COMSOL achieved this by applying the steady state Navier-Stokes and continuity equations for incompressible flows with no external forces; in this case:

$$\nabla \cdot \overline{u} = 0 \tag{2}$$

$$(\overline{u} \cdot \nabla)\overline{u} = -\nabla p + \nabla \cdot (\mu\, (\nabla \overline{u} + (\nabla \overline{u})^T)) \tag{3}$$

where $\overline{u}$ is the fluid velocity vector, and p is the absolute pressure. A similar approach was used to solve for fluid flow in TPMS structures in Ouda et al [16].

Boundary conditions. The inlet boundary condition was uniform laminar normal flow at a prescribed velocity, u_{in}. The outlet boundary condition set the pressure at the outlet to zero. At the air-TPMS interfaces a no slip boundary condition was applied. The four faces on the outside of the fluid domain running parallel to fluid flow were defined to be symmetric. The symmetry boundary condition prevents flow from leaking outside of the fluid domain by applying the following equation:

$$\overline{u} \cdot \hat{n} = 0 \tag{4}$$

where $\hat{n}$ is the unit normal vector.

Numerical modeling. A COMSOL Physics Controlled mesh was generated. The physics-controlled mesh automatically set the minimum and maximum element sizes and element growth rate, the curvature facture as well as the resolution of narrow regions [17]. Mesh size was set to "fine" (about 700k for both elements and DOFs) for good balance between performance and accuracy. A similar meshing scheme was used in Boulahrouz et al. [18] as well as Behi et al. [19]. The COMSOL stationary solver with relative tolerance was employed. The relative tolerance feature in COMSOL defaults to 0.01 which was deemed to be sufficient.

3. RESULTS AND COMMENTS

3.1 Data reduction Pressure drop in air flowing through Gyroid-type structures was first predicted employing CFD in COMSOL. Foams having ε = 0.70, 0.75, 0.80, 0.85, 0.90 porosities and d_c = 2.0, 3.0, 4.0, 5.0 mm cell sizes were investigated; the inlet velocities of the air flowing through the foams were u_{in} = 0.01, 0.03, 0.05, 0.10, 0.20, 0.50, 0.70, 1.0, 1.5, 2.0, 2.5 m/s. Very small Reynolds numbers have been investigated in order to appreciate Darcian regime, which is widely known to usually occur for Reynolds numbers in between 1 and 10. Pressure drop per unit length, where the cell size is the unit length, was predicted from CFD simulations, that allowed to derive the following correlation

$$\frac{\Delta p}{d_c} = a\, u_{in} + b\, u_{in}^2 \tag{5}$$

where the coefficients a and b were evaluated via a least square fit, using MATLAB. For the sake of exemplification, the pressure drop per unit length as a function of the inlet velocity, for ε = 0.75 and d_c = 4.0 mm, for both computations and regression from Eq. (5), are presented in Fig. 2. As it was to be expected, the regressed function, with $r^2 > 0.99$, represents very well the simulated values.

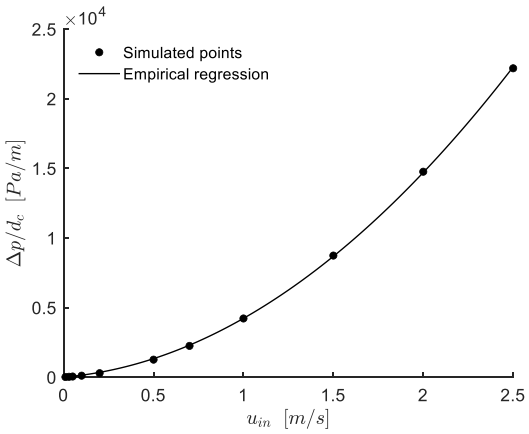

Fig. 2 Pressure drop per unit length *vs*. the air inlet velocity, for $\varepsilon = 0.75$ and d_c = 4.0 mm.

The permeability, *K*, and the Forchheimer coefficient, C_F, in a homogeneous isotropic porous medium, fully saturated with a steady state unidirectional Newtonian incompressible flow, are usually correlated with the pressure drop by the Forchheimer extended Darcy's equation for pressure drop:

$$\frac{\Delta P}{L} = \frac{\mu}{K}\, u_{in} + \rho\, C_F\, u_{in}^2 \tag{6}$$

where the first term accounts for the viscous effects (Darcian regime, Re $\leq$ 1) and the second term refers to the inertial effects (Forchheimer regime Re >> 1).
Therefore, matching Eqs.(5) and (6), one obtains:

$$K = \frac{\mu}{a} \tag{7}$$

$$C_F = \frac{b}{\rho} \tag{8}$$

3.2 Air velocity and pressure drop

Velocity field and iso-pressure contours, for ε = 0.90, u_{in} = 1.0 m/s, d_c = 3.0 mm, are presented in Figs. 3a and 3b, respectively. Figure 3a shows that the fluid velocity increases as the free section decreases and vanishes where the fluid impacts the solid surface. The figure also shows that the velocity increases with a factor of about 4 as well and the pressure drop increases too when the cross sections become very small. A similar behavior is exhibited in Fig. 3b, where high pressure drops occur when the structures are employed as heat transfer enhancers [20]. The figure exhibits a rapidly dropping pressure field, with an about 10 kPa/m pressure drop. Similar considerations as those made for Fig. 3a can be made with reference to open cell foams [20].

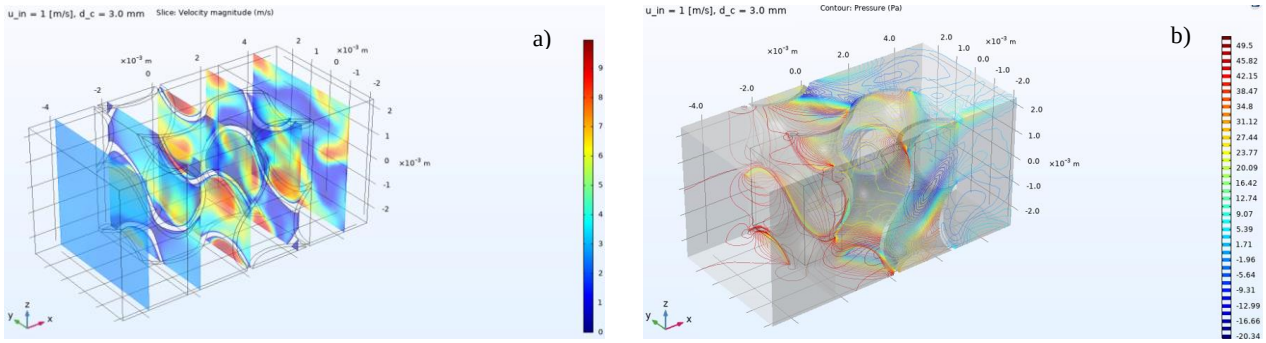

Fig. 3 (a) Velocity fields [m/s] and (b) iso-pressure contours [Pa] for ε = 0.90, u_{in} = 1.0 m/s, d_c =3.0 mm.

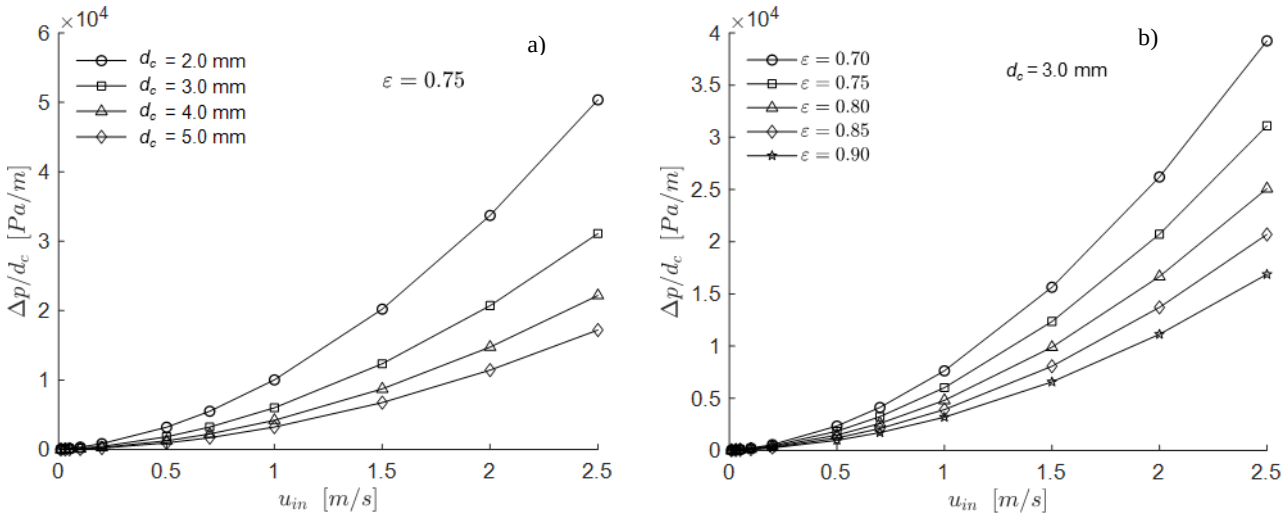

Fig. 4 Pressure drop per unit length *vs.* the air inlet velocity, for a) $\varepsilon = 0.75$ and different cell sizes; b) d_c = 3.0 mm and different porosities.

The pressure drop per unit length as a function of the air inlet velocity, for $\varepsilon = 0.75$ and different cell sizes as well as for d_c = 3.0 mm and different porosities, is presented in Figs. 4a and 4b, respectively. Both figures point out how the decrease in the free section of the foam, due to the decrease both in the cell size and in the porosity, makes the pressure drop larger. This was already noticed in Fig. 3a, where the effects of decreasing the cross section on the velocity, where highlighted. The comparison of the effects of cell size (Fig. 4a) with those of porosity (Fig. 4b) on the pressure drop shows that cell size has larger effects than porosity. This is also observed in similar structures, such as open cell foams [20], where the cell size affects the pressure drop much more than porosity. It is also worth remarking that something really similar occurs in laminar flow in channels, where pressure drop are generally inversely proportional to the square of the diameter, at equal velocity and channel length.

3.3 Permeability and Forchheimer coefficient correlations

The permeability, evaluated by means of Eq. (7), as a function of the cell size, for different porosities, as well as a function of the porosity, for different cell sizes, is presented in Figs. 5a and 5b, respectively. The figures exhibit marked increases in the permeability at increasing cell sizes and porosities. From a physical point of view, the increase in the permeability is due to the increasing area of the free section available for the fluid at increasing either the cell size or the porosity.

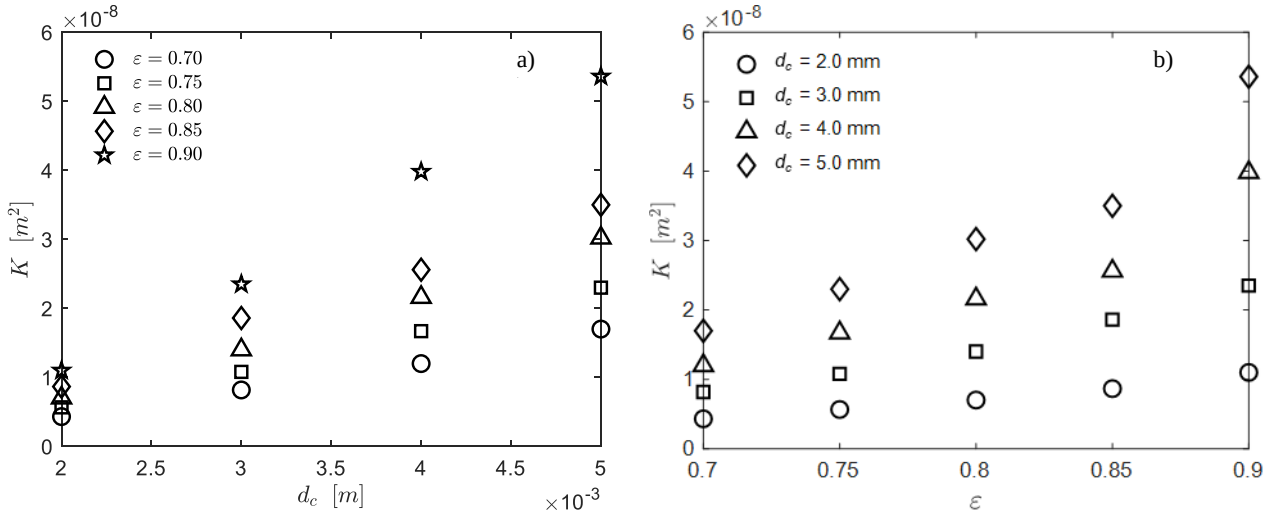

Fig. 5. Permeability *vs.* a) the cell size, for different porosities; b) the porosity, for different cell sizes.

Finding correlations among permeability in porous media and their morphological characteristics, such as cell size and porosity, is a challenging task, since they are strongly dependent on the structure of the material [2]. As far as TPMS structures are concerned, various models describing the permeability behavior of solid-based TPMS structures have been reported in the literature [12, 21]. The above cited authors, after choosing the cell size, correlated the permeability with the porosity, a morphological characteristic that affects the medium permeability. As a matter of fact, the above referred models are quite limiting since they don't account for different values of the cell sizes, that is widely known to be among the parameters that mostly characterize a porous material [2]. In the following the permeability is correlated with the porosity by using two regression parameters, *C* and *n* [13]:

$$K = C\,\varepsilon^{n} \tag{9}$$

Asbai-Ghoudan et al. [13] proposed a regression method to account for the dependence of the permeability on the cell size in various TPMSs. Herein their approach was applied to the investigated TPMS structure. First of all, we recall the following relationship between the permeability and the cell size, proposed by Kaviany [2] for a porous media conduit model:

$$K = f(\varepsilon)\,d_c^2 \tag{10}$$

with $f(\varepsilon)$ a function which depends on the geometry of the porous material. The model in [2] was used since the regular cellular structure with connected pores of the investigated Gyroid structure is similar to that of other porous materials. The function $f(\varepsilon)$ needs to be calibrated in order to take into account the dependence of permeability on the porosity.

The function $f(\varepsilon)$, that depends on the porosity, was derived from a conventional fitting analysis performed on all the available data. Assuming a linear variation of the coefficient, the permeability can be expressed via a regression analysis as follows:

$$K = (A_1\,\varepsilon - A_2)\,d_c^2 \tag{11}$$

with $A_1 = 7.13\cdot10^{-3}$, $A_2 = 4.35\ 10^{-3}$ and $r^2 > 0.95$. The dependence of $f(\varepsilon)$ on the porosity is presented in Fig. 6. It is worth noticing how the linear regression fits well with the simulated points.

In order to validate the assumption of permeability to be proportional to the cell size, the permeability as a function of the cell size, for $\varepsilon = 0.75$, is reported in Fig. 7, which exhibits a fairly good agreement between the empirical regression and the simulated points.

The Forchheimer coefficient, evaluated by means of Eq. (8), as a function of the cell size, for different porosities, as well as a function of the porosity, for different cell sizes, is presented in Figs. 8a and 8b, respectively. One can remark that the Forchheimer coefficient decreases at increasing porosity and cell size. This occurs because drag

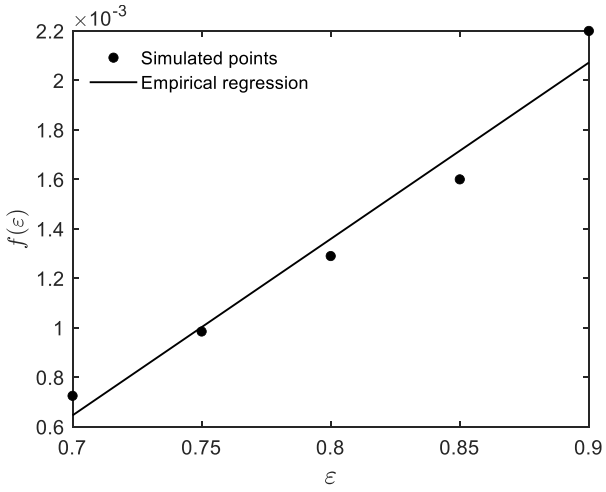

Fig. 6. Function $f(\varepsilon)$ *vs*. the porosity.

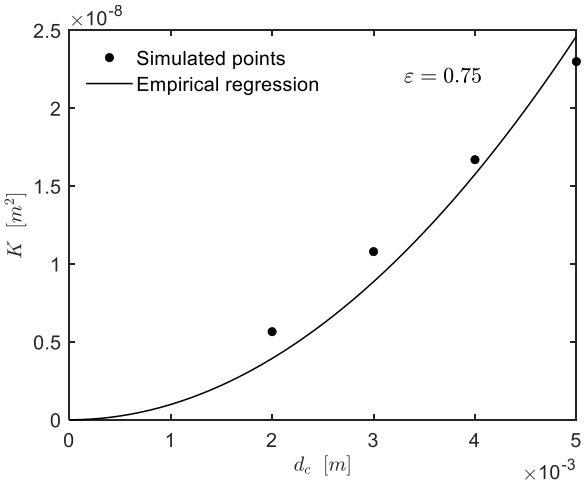

Fig.7 Permeability *vs*. the cell size, for $\varepsilon = 0.75$.

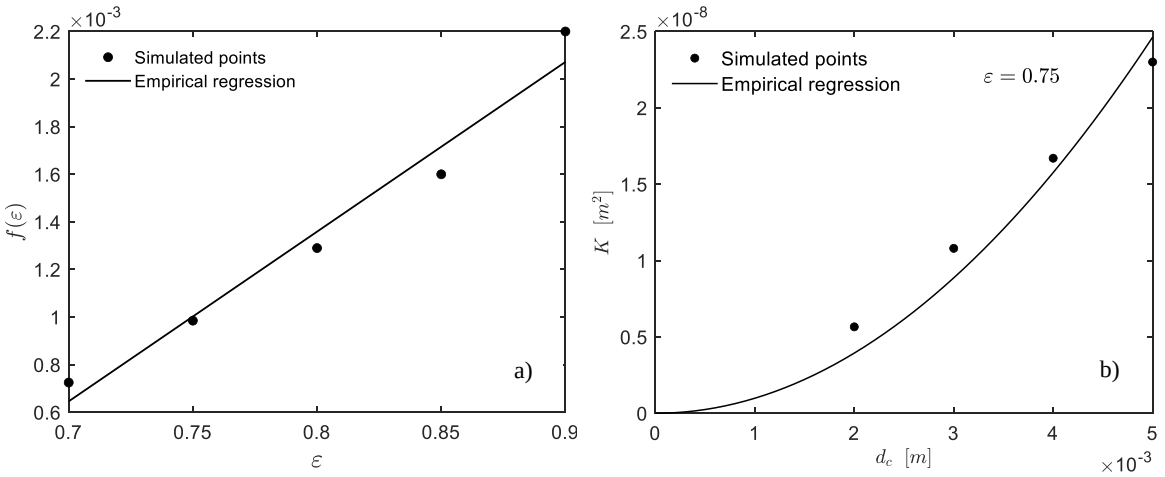

Fig. 8 Forchheimer coefficient *vs*. a) cell size, for different porosities; b) porosity, for different cell sizes

forces increase both with smaller porosities, that make more surface area available, and with smaller cell sizes. The latter behavior is similar to that of the friction factor and the diameter in channels. In a similar way, inertial factors, which are proportional to the Forchheimer coefficient via the square root of the permeability, might decrease at very high porosities because of variations in the strut shape [22].
Exhaustive correlations for the Forchheimer coefficient in porous materials, as well as for TPMS, are limited. Therefore, herein the following power-law correlation among the Forchheimer coefficient, the porosity and the cell size was assumed:

$$C_F = a_1 \, \varepsilon^{b_1} \, d_C^{c_1} \tag{12}$$

where the coefficients, a_1 = 2.11 m^{-2}, b_1 = 3.30, c_1 = 1.12 were obtained by means of a non-linear regression analysis, with r^2 = 0.99. The Forchheimer coefficient as a function of the cell size and the porosity is plotted in Fig. 9. According to the high value of the regression coefficient, we can notice that the regressed surface fairly fits with the simulated points.

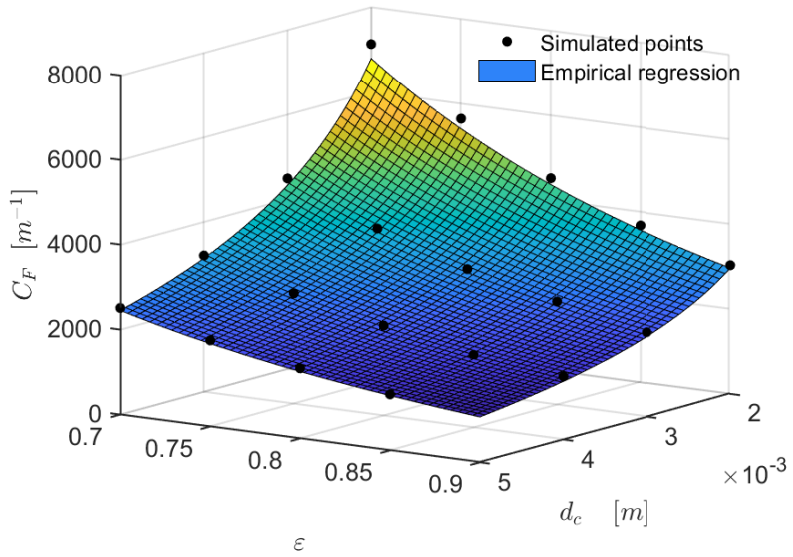

Fig. 9 The Forchheimer coefficient *vs*. the cell size and the porosity.

4. CONCLUSIONS

In this study, permeability and Forchheimer coefficient for a Gyroid TPMS have been correlated with morphological characteristics of cellular materials, such as porosity and cell sizes. Computations have been done by employing a CFD pore scale model, and results in terms of pressure drop have been reduced to obtain permeability and Forchheimer coefficient for each of the investigated structures. Results showed that the impact of cell size on pressure drop is far higher than that of porosity. It was found that the permeability generally increases with both cell size and porosity; it was also shown that it is reasonable to correlate it with the cell size by a quadratic law and with the porosity by a linear regression. A power law has been employed to correlate Forchheimer coefficient with the structural parameters of the Gyroid TPMS, showing that, thanks to the high coefficient of determination obtained, the power law assumption was far reasonable. This study will be really helpful in designing TPMS-based devices, such as heat exchangers.

ACKNOWLEDGMENTS

This work was carried out within a Cooperation Agreement between the University of Connecticut (USA) and the Università degli Studi Federico II (Italy) and was supported by Italian Government MIUR Grant No. PRIN-2017F7KZWS.

NOMENCLATURE

Latin symbols

a, b	pressure drop regression coefficients (Eq.5)	d_c	cell size (m)
a_1, b_1, c_1	Forchheimer regression coefficients (Eq.12)	K	permeability (m^2)
A_1, A_2	porosity regression coefficients (Eq.11)	***Greek symbols***	
C, n	regression parameters (Eq.9)	ε	porosity (-)
C_F	Forchheimer coefficient (m^{-1})	$\phi(x, y, z)$	TPMS function (-)

REFERENCES

[1] Dukhan, N., *Metal Foams: Fundamentals and Applications*, DEStech Publications, Inc., (2013).
[2] Kaviany, M., *Principles of Heat Transfer in Porous Media*, Springer Science & Business Media, (2012).
[3] Edouard, D., Lacroix, M., Huu, C.P., Luck, F., "Pressure drop modeling on solid foam: State-of-the art correlation," Chem. Engin. J., 144(2), pp. 299-311, (2008).
[4] Boomsma, K., Poulikakos, D., Ventikos, Y. "Simulations of flow through open cell metal foams using an idealized periodic cell structure,". Int. J. Heat Fluid Flow, 24(6),pp. 825-834, (2003).
[5] Du Plessis, J.P., Masliyah, J.H., "Mathematical modelling of flow through consolidated isotropic porous media," Transp. Porous Media, 3(2), 145-161, (1988).
[6] Attarzadeh, R., Rovira, M., Duwig, C., "Design analysis of the "Schwartz D" based heat exchanger: A numerical study," Int. J. Heat Mass Transf., 177, pp. 121415, (2021).
[7] Schoen, R.M., "Uniqueness, symmetry, and embeddedness of minimal surfaces," J. Diff. Geom., 18(4), pp.791-809, (1983).
[8] Ali, D., Ozalp, M., Blanquer, S.B., Onel, S. "Permeability and fluid flow-induced wall shear stress in bone scaffolds with TPMS and lattice architectures: A CFD analysis," Eur. J. Mechanics-B/Fluids, 79, 376-385, (2020).
[9] Castro, A.P.G., Pires, T., Santos, J E., Gouveia, B.P., Fernandes, P.R., "Permeability versus design in TPMS scaffolds." Materials, 12(8), 1313, (2019).
[10] Kaur, I., Singh, P., "Flow and thermal transport characteristics of Triply-Periodic Minimal Surface (TPMS)-based gyroid and Schwarz-P cellular materials," Num. Heat Transf., Part A: Applications, 79(8), 553-569, (2021).
[11] Cheng, Z., Xu, R., Jiang, P.X., " Morphology, flow and heat transfer in triply periodic minimal surface based porous structures." Int. J. Heat Mass Transf., 170, 120902, (2021).
[12] Zhianmanesh, M., Varmazyar, M., Montazerian, H., "Fluid permeability of graded porosity scaffolds architectured with minimal surfaces, "ACS Biom. Science Engin., 5(3), 1228-1237, (2019).
[13] Asbai-Ghoudan, R., de Galarreta, S.R., Rodriguez-Florez, N., "Analytical model for the prediction of permeability of triply periodic minimal surfaces," J. Mechan. Behavior Biom. Mat., 124, 104804, (2021).

[14] Al‐Ketan, O., Abu Al‐Rub, R.K., "MSLattice: A free software for generating uniform and graded lattices based on triply periodic minimal surface," Mat. Design Proces. Comm., 3(6), e205, (2021).
[15] Wu, Z., Caliot, C., Flamant, G., Wang, Z., "Numerical simulation of convective heat transfer between air flow and ceramic foams to optimise volumetric solar air receiver performances," Int. J. Heat Mass Transf., 54(7-8), 1527-1537, (2011).
[16] Ouda, M., Al-Ketan, O., Sreedhar, N., Ali, M.I.H., Al-Rub, R.K.A., Hong, S., Arafat, H.A., "Novel static mixers based on triply periodic minimal surface (TPMS) architectures," J. Envir. Chem. Engin., 8(5), 104289, (2020).
[17] Dickinson, E.J., Ekström, H., Fontes, E., "COMSOL Multiphysics®: Finite element software for electrochemical analysis. A mini-review," Electrochem. Comm., 40, 71-74, (2014).
[18] Boulahrouz, S., Avenas, Y., Chehhat, A., "CFD simulation of heat transfer and fluid flow within metallic foam in forced convection environment," Mech. Mechanical Engin. 21(3), 611-635, (2017).
[19] Behi, H., Karimi, D., Youssef, R., Suresh Patil, M., Van Mierlo, J., Berecibar, M., "Comprehensive passive thermal management systems for electric vehicles," Energies, 14(13), 3881, (2021).
[20] Wu, Z., Caliot, C., Bai, F., Flamant, G., Wang, Z., Zhang, J., Tian, C., "Experimental and numerical studies of the pressure drop in ceramic foams for volumetric solar receiver applications," Applied Energy, 87(2), 504-513, (2010).
[21] Davoodi, E., Montazerian, H., Esmaeilizadeh, R., Darabi, A.C., Rashidi, A., Kadkhodapour, J., Toyserkani, E., "Additively manufactured gradient porous Ti–6Al–4V hip replacement implants embedded with cell-laden gelatin methacryloyl hydrogels," ACS Appl. Mat. Interfaces, 13(19), 22110-22123, (2021).
[22] Bhattacharya, A., Calmidi, V.V., Mahajan, R. L., "Thermophysical properties of high porosity metal foams," Int. J. Heat Mass Transf., 45(5), 1017-1031, (2002).